Passivity-based Linear Feedback Control of Permanent Magnetic Synchronous Generator based Wind Energy Conversion System: Design and Analysis

Bo Yang [1], Tao Yu [2,*], Hongchun Shu [1], Dalin Qiu [1], Yuming Zhang [1], Pulin Cao [1], and Lin Jiang [3]

[1] Faculty of Electric Power Engineering, Kunming University of Science and Technology, 650500 Kunming, China;
[2] College of Electric Power, South China University of Technology, 510640 Guangzhou, China;
[3] Department of Electrical Engineering & Electronics, University of Liverpool, Liverpool, L69 3GJ, United Kingdom.
* Correspondence: taoyu1@scut.edu.cn, Tel.: +86-130-020-88518

Abstract: This paper designs a passivity-based linear feedback control (PBLFC) scheme of a permanent magnetic synchronous generator (PMSG) based wind energy conversion system (WECS), which attempts to achieve a maximum power point tracking (MPPT) at generator-side voltage source converter (VSC) and enhance fault ride-through (FRT) capability at grid-side VSC simultaneously. A storage function is constructed based on the passivity theory, in which the actual role of each term is meticulously investigated while the beneficial ones are remained so as to significantly improve the transient responses. Then, an auxiliary input is employed in the form of linear feedback control to ensure a desired tracking error convergence. Moreover, the closed-loop system stability is thoroughly analyzed, together with a detailed physical interpretation of the storage function. Three case studies are undertaken including step change of wind speed, stochastic wind speed variation, and FRT. Simulation results verify that the proposed approach can effectively achieve MPPT and dramatically improve the FRT capability under various operation conditions against that of vector control (VC) and feedback linearization control (FLC).

Keywords: PMSG; passivity-based linear feedback control; maximum power point tracking; fault ride-through; storage function

Nomenclature

Variables		ω_g	angular speed of grid voltage
v_{wind}	wind velocity	R_g	equivalent resistance of grid
ρ	air density	L_g	equivalent inductance of grid
C_P	power coefficient	E_d,E_q	dq-axis peak value of grid voltage
λ	tip-speed-ratio	C	DC-link capacitance
β	blade pitch angle	E	peak value of grid voltage
T_e	electromagnetic torque	R_s	stator resistance
T_m	mechanical torque	*Abbreviations*	
ω_e	electrical rotation speed	MPPT	maximum power point tracking
ω_m	mechanical rotation speed of turbine	PMSG	permanent magnetic synchronous generator
V_{d1},V_{q1}	dq-axis stator voltages	VC	vector control
i_{d1},i_{q1}	dq-axis currents of PMSG	WECS	wind energy conversion system
I_{dc1},I_{dc1},I_{dc2}	DC-link currents	FRT	fault ride-through
V_{dc}	DC-link voltage	VSC	voltage source converter
V_{d2},V_{q2}	dq-axis voltages of grid-side VSC	PID	proportional-integral-derivative
i_{d2},i_{q2}	dq-axis currents of grid-side VSC	FLC	feedback linearization control
System parameters		PBLFC	passivity-based linear feedback control
L_d,L_q	dq-axis inductances of generator-side VSC	AC	alternating current
p	the number of pole pairs	DC	direct current
R	turbine radius	*Control parameters of PBLFC*	
J_{tot}	total inertia of drive train	α_{11}, α_{21}, α_{22}	linear feedback control gains of generator-side VSC
D	viscous damping coefficient	α'_{11}, α'_{12}, α'_{21}	linear feedback control gains of grid-side VSC

1. Introduction

How to meet the ever-growing energy demand is definitely one of the most paramount and urgent agenda of the twenty-first century [1]. Disruption of the ecological balance by fossil fuels and their imminent depletion has lead energy demand a quite severe challenge for the globe. Currently, clean and renewable energy resources are gaining enormous attentions as a powerful alternative to tackle the emerging energy crisis and continuous environmental deterioration, including hydro, wind, solar, biomass, etc. [2].

Among various forms of renewable energy, wind energy conversion system (WECS) plays a very crucial role and becomes very popular due to its promising merits of cleanness, abundance, and wide distribution [3]. At present, variable speed wind turbine systems are mainly based on either doubly-fed induction generator (DFIG) [4] or permanent magnetic synchronous generator (PMSG) [5]. In the past decade, the worldwide deployment of PMSG has been considerably boomed thanks to its elegant features of simple structure, efficient energy production, gearless construction, self-excitation, and low noises.

So far, the control system of PMSG usually requires itself to achieve both maximum power point tracking (MPPT) [6] at various wind speeds and to realize fault ride-through (FRT) [7] in the presence of grid faults. Currently, vector control (VC) associated with proportional-integral (PI) or proportional-integral-derivative (PID) loops has been widely used thanks to its structure simplicity and high reliability [8]. In general, it is very powerful to achieve the desired performance over a fixed set of operation points as the control gains are mainly determined through one-point linearization of the original nonlinear systems. Nevertheless, VC cannot maintain a consistent control performance when the operation conditions vary, or might even lead to system instability. Expectedly, such fundamental inadequacy will become much severer when facing the fast time-varying stochastic wind speed variation and different grid voltage dips.

In order to tackle the inherent flaws of VC, an enormous variety of nonlinear adaptive/robust control schemes have been proposed for PMSG in the past decade. A feedback linearization control (FLC) was designed for PMSG to achieve MPPT, which offers a global control consistency via full nonlinearities compensation [9]. For the purpose of robustness improvement of PMSG, an enhanced exponential reaching law based sliding-mode control (SMC) was developed for PMSG to reduce the malignant chattering issues and to improve the total harmonic distortion property [10]. Moreover, reference [11] reported a robust nonlinear predictive control (RNPC) to realize MPPT and to charge battery despite the presence of disturbances. In work [12], a nonlinear Luenberger-like observer was applied to estimate the mechanical variables by only the measurement of electrical variables of PMSG to achieve MPPT. On the other hand, a perturbation estimation based nonlinear adaptive control (NPC) was developed for PMSG to enhance the FRT capability under different disturbances and uncertainties [13]. Besides, an interval type-2 fuzzy logic control was devised to improve FRT capability by taking into account the nonlinear relationship between the generator speed and the DC-link voltage [14]. Meanwhile, an active disturbance rejection control (ADRC) was proposed to compensate the lumped disturbance efficiently thus MPPT could be achieved [15].

Generally speaking, the aforementioned approaches mainly regard the control system design of PMSG as a pure mathematical problem, while the physical property or unique features of PMSG are somehow unaddressed. Passivity-based control (PBC) provides a powerful tool to systematically analyze the essential physical property of engineering problems. It normally treats a dynamical system as an energy transmission device, while the controller is viewed as another energy exchanging device which enables the overall energy of the controlled system to be desirably reshaped, upon dynamical interconnection, such that a satisfactory closed-loop system performance could be realized [16]. Based on an online wind speed estimator, reference [17] developed an Euler-Lagrange model of PMSG to achieve MPPT using PBC, of which the asymptotic stability of the equilibrium is strictly proved. In addition, an interconnection and damping assignment passivity-based control (IDA-PBC) was developed to realize MPPT with the help of a mechanical torque estimator [18]. Besides, a port-controlled Hamiltonian dissipation (PCHD) based model was employed for PMSG to achieve MPPT via energy dissipation [19]. A passivity-based sliding-mode control (PB-SMC) [20] was developed to combine the merits of PBC and SMC [21] for a PMSG to achieve MPPT, such that a great robustness can be provided in the presence of various uncertainties. In references [22] and [23], port-controlled Hamiltonian (PCH) based control were proposed to improve the dynamical response of PMSG under different grid faults. Besides, literatures [24] and [25] presented a passivity/SMC scheme for solar/wind hybrid systems, which can achieve a satisfactory control performance under various operation conditions. Moreover, work [26] and [27] systematically devised PBC for PMSG based WECS using Euler-Lagrange representation, which can accelerate the tracking performance thus an efficient MPPT could be resulted in.

The contributions and motivations of this paper can be highlighted as follows:

- The highly-stochastic operation conditions and complex nonlinearities of PMSG motivate this paper to design a passivity-based linear feedback control (PBLFC), which can fully exploit the physical properties of PMSG to realize an improved control performance by carefully retaining the beneficial terms of PMSG;
- Compared to the authors' previous work [20] which has a relatively complicated control structure. It motivates this paper to design PBLFC strategy with a simpler control structure, such that it is easier to be implemented;
- Compared to publications [20-27] which handle either MPPT or FRT separately. It motivates this paper to design a completed PBC scheme for a PMSG based wind energy conversion systems (WECS) with the consideration of both MPPT and FRT;
- An auxiliary linear feedback control framework is employed to guarantee a desired tracking error convergence, which is easier to be understood and accepted by industry. Moreover, the closed-loop system is thoroughly analyzed to investigate the roots and properties of the passivized system.

Case studies are carried out to evaluate the control performance of the proposed approach against that of VC and FLC.

The rest of the paper is organized as follows: Section 2 develops the PMSG based WECS model. Then, PBLFC is designed for PMSG based WECS in Section 3 while the closed-loop system is thoroughly analyzed in Section 4. Comprehensive case studies are carried out in Section 5. Finally, conclusions are summarized in Section 6.

2. Modelling of PMSG based Wind Energy Conversion System

Fig. 1 illustrates the configuration of a PMSG based WECS with back-to-back voltage source converter (VSC), in which the wind energy captured by a variable speed wind turbine is delivered to a gearless PMSG. In particular, the produced active power and reactive power of the generator is controlled by a generator-side VSC, meanwhile the active power transmission and DC-link voltage regulation is realized by a grid-side VSC. Here, two VSCs are controlled independently while the dynamics of the PMSG and the power grid is fully decoupled via the DC-link [12].

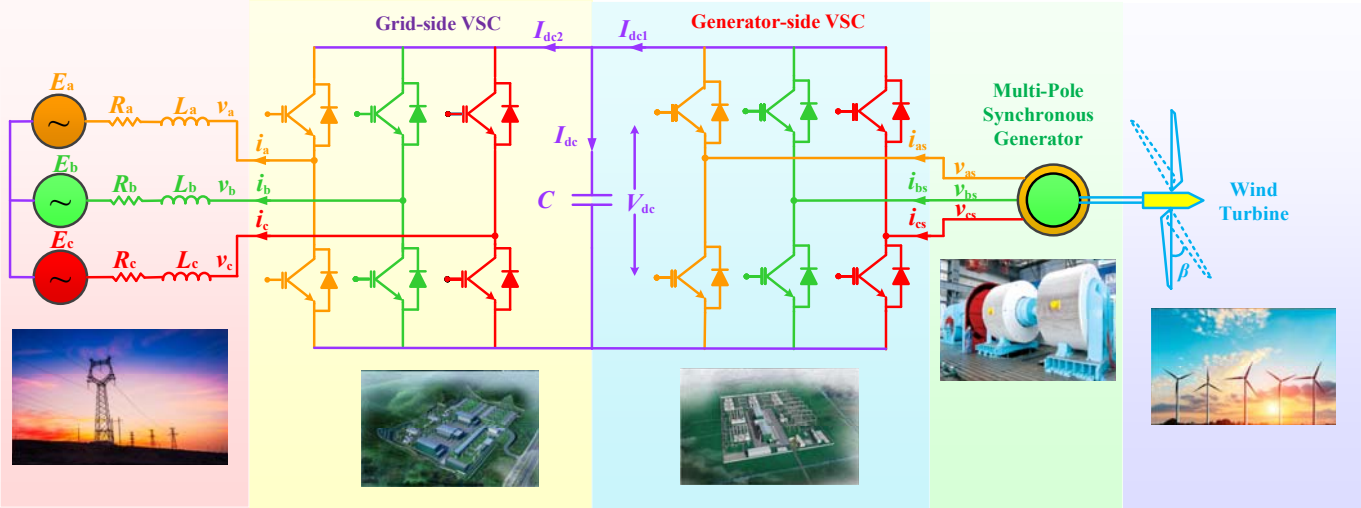

Figure 1. The configuration of a PMSG based wind energy conversion system.

2.1. *Generator-side VSC modelling*

The aerodynamics of wind turbine is normally described by a power coefficient $C_p(\lambda,\beta)$, which is usually an algebraic function of both blade pitch angle β and tip-speed-ratio λ, with λ being defined by [9,28]

$$\lambda = \frac{\omega_m R}{v_{wind}} \tag{1}$$

where ω_m denotes the mechanical rotation speed of wind turbine and v_{wind} represents the wind speed; R is the blade radius of wind turbine, respectively. According to the wind turbine dynamics, a generic equation employed to describe the power coefficient $C_p(\lambda,\beta)$ can be written as

$$C_p(\lambda,\beta) = c_1\left(\frac{c_2}{\lambda_i} - c_3\beta - c_4\right)e^{-\frac{c_5}{\lambda_i}} \tag{2}$$

with

$$\frac{1}{\lambda_i} = \frac{1}{\lambda+0.08\beta} - \frac{0.035}{\beta^3+1} \tag{3}$$

where the coefficients c_1 to c_5 are selected as c_1=0.22, c_2=116, c_3=0.4, c_4=5, and c_5=12.5, respectively [12,28].

Moreover, the mechanical power extracted by the wind turbine from the wind energy is calculated by

$$P_m = \frac{1}{2}\rho\pi R^2 C_p(\lambda,\beta)v_{wind}^3 \tag{4}$$

where ρ is the air density. Note that during MPPT the wind turbine only operates in the sub-rated speed range while its pitch control is deactivated for the whole operation of PMSG.

The PMSG dynamics in the d-q reference frames are expressed as follows [9,28]:

$$V_{d1} = R_s i_{d1} + L_d\frac{di_{d1}}{dt} - \omega_e L_q i_{q1} \tag{5}$$

$$V_{q1} = R_s i_{q1} + L_q\frac{di_{q1}}{dt} + \omega_e(L_d i_{d1} + K_e) \tag{6}$$

$$T_e = p[(L_d - L_q)i_{d1}i_{q1} + i_{q1}K_e] \tag{7}$$

where V_{d1} and V_{q1} are the stator voltages in the d-q axis; i_{d1} and i_{q1} are the currents of PMSG in the d-q axis; R_s is the stator resistance; L_d and L_q are d-q axis inductances; $\omega_e = p\omega_m$ is the electrical rotation speed; K_e is the permanent magnetic flux given by the magnets; and p is the number of pole pairs, respectively.

The dynamics of mechanical shaft system and mechanical torque of PMSG are given by [9,28]

$$J_{tot}\frac{d\omega_m}{dt} = T_m - T_e - D\omega_m \tag{8}$$

$$T_m = \frac{1}{2}\rho\pi R^5\frac{C_p(\lambda,\beta)}{\lambda^3}\omega_m^2 \tag{9}$$

where J_{tot} is the total inertia of the drive train which equals to the summation of wind turbine inertia constant and generator inertia constant; D is the viscous damping coefficient which equals to zero in this paper; T_m is the mechanical torque of wind turbine, respectively. Moreover, active power is calculated as $P_e = T_e\omega_e$ where T_e represents the electromagnetic torque.

2.2. *Grid-side VSC modelling*

Only the balanced condition is considered, e.g., the three phases have identical parameters and their voltages and currents have the same amplitude while each phase shifts 120° between themselves. Moreover, it assumes the converter losses are ignored [13].

The dynamics of grid-side VSC in the d-q reference frames are described as [13]

$$E_d = R_g i_{d2} + L_g\frac{di_{d2}}{dt} - \omega_g L_g i_{q2} + V_{d2} \tag{10}$$

$$E_q = R_g i_{q2} + L_g\frac{di_{q2}}{dt} + \omega_g L_g i_{d2} + V_{q2} \tag{11}$$

$$\frac{dV_{dc}}{dt} = \frac{I_{dc1}}{C} - \frac{3E_d i_{d2}}{2CV_{dc}} \tag{12}$$

where E_d and E_q are the d-q axis components of three-phase grid voltages (E_a, E_b, E_c); V_{d2} and V_{q2} denote the d-q axis component of three-phase grid-side VSC voltages (v_a, v_b, v_c); i_{d2} and i_{q2} represent the d-q axis components of three-phase grid currents (i_a, i_b, i_c); R_g and L_g mean the equivalent resistance and inductance between grid-side VSC and the high voltage terminals of the grid-connected transformer; C represents the DC-link capacitor and ω_g is the angular speed of grid voltage; I_{dc} denotes the DC-link current with V_{dc} being the voltage across it; $I_{dc1} = P_e/V_{dc}$ is the generator-side DC-link current while I_{dc2} is the grid-side DC-link current, respectively. Note that the d-axis of the synchronous rotating frame is aligned with the grid voltage vector, which results in $E_q = 0$ and $E_d = E$, where E denotes the peak value of the grid voltage.

3. PBLFC Design of PMSG

3.1. *Passivity-based control*

The objective of PBC is to passivize a dynamical system with a storage function which has a minimum at the desired equilibrium point, thus it can effectively reshape the system energy and assign a closed-loop energy function equal to the difference between the energy of the system and the energy supplied by the controller.

Consider a dynamical nonlinear system represented with the following general model

$$\begin{cases}\dot{x} = f(x,u)\\ y = h(x,u)\end{cases} \tag{13}$$

where $x \in \mathcal{R}^n$ is the system state vector. $u \in \mathcal{R}^m$ and $y \in \mathcal{R}^m$ represent the input and output, respectively.

The energy balancing can be written as follows [16]:

$$\underbrace{H[x(t)] - H[x(0)]}_{\text{stored}} = \underbrace{\int_0^t u^{\mathrm{T}}(s)y(s)\mathrm{d}s}_{\text{supplied}} - \underbrace{d(t)}_{\text{dissipated}} \tag{14}$$

where $H(x)$ is the storage function, and $d(t)$ is a nonnegative function that characterizes the dissipation effects in practical engineering problems, such as friction and heat. Undoubtedly, energy balancing is a universal property of physical systems, which captures a very broad range of applications that include nonlinear and time-varying dynamics.

System (13) is defined to be output strictly passive if there exists a continuously differentiable positive semi-definite function $H(x)$, such that

$$u^{\mathrm{T}}y \geq \frac{\partial H}{\partial x}f(x,u) + \zeta y^{\mathrm{T}}y, \forall (x,u) \in \mathcal{R}^n \times \mathcal{R}^m \tag{15}$$

where $\zeta > 0$. In order to obtain the asymptotic stability, the following Lemma 1 is needed.

Lemma 1 [16]**.** *Consider system (13), The origin of the uncontrolled system $\dot{x} = f(x,0)$ is asymptotically stable if the system is output strictly passive and zero-state detectable with a positive definite storage function $H(x)$. Moreover, if the storage function $H(x)$ is radially unbounded then the origin is globally asymptotically stable.*

If system (15) is not passive, but there exists a positive definite storage function $H(x)$ and a feedback control law $u = \beta(x) + kv$ such that $\dot{H} \leq vy$, then the feedback system is passive. As a result, the feedback passivation can be used as a preliminary step in a stabilization design due to the additional output feedback

$$v = -\phi(y) \tag{16}$$

where $\phi(y)$ is a sector-nonlinearity satisfying $y\phi(y) > 0$ for $y \neq 0$ and $\phi(0)=0$, can achieve $\dot{H} \leq -y\phi(y) \leq 0$.

Here, different control framework could be employed for the additional input to accomplish various PBC design. This paper adopts the linear feedback control (LFC) form due to its high reliability and simple structure.

3.2 Generator-side VSC control design

The control design of generator-side VSC aims to achieve MPPT at sub-rated wind speed. Here, the pitch angle is taken to be $\beta = 2°$, the optimal tip-speed-ratio $\lambda^* = 7.4$ while maximum power coefficient $C_{\mathrm{p}}^* = 0.4019$ [9,24]. Additionally, x^* denotes the reference of variable x throughout the whole paper.

Define the tracking error $e=[e_1,\ e_2]^{\mathrm{T}}=[i_{\mathrm{d1}}\text{-}i_{\mathrm{d1}}^*,\ \omega_{\mathrm{m}}\text{-}\omega_{\mathrm{m}}^*]^{\mathrm{T}}$, with i_{d1}^* and ω_{m}^* being the references of d-axis current and mechanical rotation speed, respectively. Differentiate the tracking error until the control input $u=[u_1,\ u_2]^{\mathrm{T}}=[V_{\mathrm{d1}},\ V_{\mathrm{q1}}]^{\mathrm{T}}$ appears explicitly, gives

$$\begin{bmatrix}\dot{e}_1\\ \ddot{e}_2\end{bmatrix} = \begin{bmatrix}f_1(x)\\ f_2(x)\end{bmatrix} + B_1(x)\begin{bmatrix}u_1\\ u_2\end{bmatrix} - \begin{bmatrix}\dot{i}_{\mathrm{d1}}^*\\ \ddot{\omega}_{\mathrm{m}}^*\end{bmatrix} \tag{17}$$

where

$$f_1(x) = -\frac{R_{\mathrm{s}}}{L_{\mathrm{d}}}i_{\mathrm{d1}} + \frac{\omega_{\mathrm{e}}L_{\mathrm{q}}}{L_{\mathrm{d}}}i_{\mathrm{q1}} \tag{18}$$

$$f_2(x) = \frac{\dot{T}_{\mathrm{m}}}{J_{\mathrm{tot}}} - \frac{pi_{\mathrm{q1}}}{J_{\mathrm{tot}}L_{\mathrm{d}}}\left(L_{\mathrm{d}} - L_{\mathrm{q}}\right)\left(-R_{\mathrm{s}}i_{\mathrm{d1}} + L_{\mathrm{q}}\omega_{\mathrm{e}}i_{\mathrm{q1}}\right) + \frac{p}{J_{\mathrm{tot}}L_{\mathrm{q}}}[K_{\mathrm{e}} + \left(L_{\mathrm{d}} - L_{\mathrm{q}}\right)i_{\mathrm{d1}}](L_{\mathrm{d}}\omega_{\mathrm{e}}i_{\mathrm{d1}} + R_{\mathrm{s}}i_{\mathrm{q1}} + \omega_{\mathrm{e}}K_{\mathrm{e}}) \tag{19}$$

with

$$B_1(x) = \begin{bmatrix}\frac{1}{L_{\mathrm{d}}} & 0\\ -\frac{pi_{\mathrm{q1}}}{J_{\mathrm{tot}}L_{\mathrm{d}}}(L_{\mathrm{d}} - L_{\mathrm{q}}) & -\frac{p}{J_{\mathrm{tot}}L_{\mathrm{q}}}[K_{\mathrm{e}} + (L_{\mathrm{d}} - L_{\mathrm{q}})i_{\mathrm{d1}}]\end{bmatrix} \tag{20}$$

The inverse of control gain matrix $B_1(x)$ can be calculated as follows:

$$B_1^{-1}(x) = \begin{bmatrix}L_{\mathrm{d}} & 0\\ -\frac{i_{\mathrm{q1}}L_{\mathrm{q}}(L_{\mathrm{d}}-L_{\mathrm{q}})}{K_{\mathrm{e}}+(L_{\mathrm{d}}-L_{\mathrm{q}})i_{\mathrm{d1}}} & -\frac{J_{\mathrm{tot}}L_{\mathrm{q}}}{p[K_{\mathrm{e}}+(L_{\mathrm{d}}-L_{\mathrm{q}})i_{\mathrm{d1}}]}\end{bmatrix} \tag{21}$$

In order to ensure the above input-output linearization to be valid, it requires control gain matrix $B_1(x)$ must be nonsingular among the whole operation range, obtains

$$\det[B_1(x)] = -\frac{p[K_{\mathrm{e}}+(L_{\mathrm{d}}-L_{\mathrm{q}})i_{\mathrm{d1}}]}{J_{\mathrm{tot}}L_{\mathrm{d}}L_{\mathrm{q}}} \neq 0 \tag{22}$$

which can be always satisfied when $K_{\mathrm{e}} \neq -(L_{\mathrm{d}}-L_{\mathrm{q}})i_{\mathrm{d1}}$.

For system (17), construct a storage function as follows:

$$H_1 = \underbrace{\frac{1}{2}(i_{\mathrm{d1}} - i_{\mathrm{d1}}^*)^2}_{\text{AC series-resistor heat}} + \underbrace{\frac{1}{2}(\omega_{\mathrm{m}} - \omega_{\mathrm{m}}^*)^2}_{\text{kinetic energy}} + \underbrace{\frac{1}{2}\left(\frac{T_{\mathrm{m}}-T_{\mathrm{e}}}{J_{\mathrm{tot}}} - \dot{\omega}_{\mathrm{m}}^*\right)^2}_{\text{acceleration torque energy}} \tag{23}$$

Here, H_1 is constructed in the form of the sum of the heat produced by d-axis current i_{d1} flowing through an AC series virtual unit resistor, kinetic energy of the mechanical shaft system, and acceleration torque energy, respectively.

Remark 1. Note that the tracking error and storage function H_1 only include the d-axis current i_{d1} and mechanical rotation speed ω_{m} while q-axis current i_{q1} is excluded. This is due to the reason that MPPT is achieved by regulating mechanical rotation speed ω_{m} (with relative degree of 2); While another goal is to regulate the reactive power which is determined by the d-axis current i_{d1} in the chosen alignment framework (with relative degree of 1). As there are only two inputs, e.g., u_1 and u_2, and the overall order of tracking error dynamics is 3, they are fully used to achieve the above two goals (2+1=3) and no more input could be adopted for the regulation of q-axis current i_{q1}. However, based on the relationship (5)-(9), q-axis current will be indirectly regulated after the d-axis current and mechanical rotation speed are all controlled.

Differentiate storage function H_1 (23) with respect to the time using Eq. (7) and Eqs. (17)-(20), yields

$$\begin{aligned}\dot{H}_1 &= (i_{\mathrm{d1}} - i_{\mathrm{d1}}^*)\left(\dot{i}_{\mathrm{d1}} - \dot{i}_{\mathrm{d1}}^*\right) + (\omega_{\mathrm{m}} - \omega_{\mathrm{m}}^*)\left(\frac{T_{\mathrm{m}}-T_{\mathrm{e}}}{J_{\mathrm{tot}}} - \dot{\omega}_{\mathrm{m}}^*\right) + \left(\frac{T_{\mathrm{m}}-T_{\mathrm{e}}}{J_{\mathrm{tot}}} - \dot{\omega}_{\mathrm{m}}^*\right)(\ddot{\omega}_{\mathrm{m}} - \ddot{\omega}_{\mathrm{m}}^*)\\ &= (i_{\mathrm{d1}} - i_{\mathrm{d1}}^*)\left(\frac{1}{L_{\mathrm{d}}}u_1 - \frac{R_{\mathrm{s}}}{L_{\mathrm{d}}}i_{\mathrm{d1}} + \frac{\omega_{\mathrm{e}}L_{\mathrm{q}}}{L_{\mathrm{d}}}i_{\mathrm{q1}} - \dot{i}_{\mathrm{d1}}^*\right) + \left(\frac{T_{\mathrm{m}}-T_{\mathrm{e}}}{J_{\mathrm{tot}}} - \dot{\omega}_{\mathrm{m}}^*\right)(-\ddot{\omega}_{\mathrm{m}}^* + \ddot{\omega}_{\mathrm{m}} + \omega_{\mathrm{m}} - \omega_{\mathrm{m}}^*)\\ &= (i_{\mathrm{d1}} - i_{\mathrm{d1}}^*)\left(\frac{1}{L_{\mathrm{d}}}u_1 - \frac{R_{\mathrm{s}}}{L_{\mathrm{d}}}i_{\mathrm{d1}} + \frac{\omega_{\mathrm{e}}L_{\mathrm{q}}}{L_{\mathrm{d}}}i_{\mathrm{q1}} - \dot{i}_{\mathrm{d1}}^*\right) + \left(\frac{T_{\mathrm{m}}-T_{\mathrm{e}}}{J_{\mathrm{tot}}} - \dot{\omega}_{\mathrm{m}}^*\right)\left\{-\ddot{\omega}_{\mathrm{m}}^* - \frac{pi_{\mathrm{q1}}}{J_{\mathrm{tot}}L_{\mathrm{d}}}\left(L_{\mathrm{d}} - L_{\mathrm{q}}\right)u_1 - \frac{p}{J_{\mathrm{tot}}L_{\mathrm{q}}}[K_{\mathrm{e}} + \left(L_{\mathrm{d}} - L_{\mathrm{q}}\right)i_{\mathrm{d1}}]u_2 + \frac{\dot{T}_{\mathrm{m}}}{J_{\mathrm{tot}}} - \frac{pi_{\mathrm{q1}}}{J_{\mathrm{tot}}L_{\mathrm{d}}}\left(L_{\mathrm{d}} - L_{\mathrm{q}}\right)\left(-R_{\mathrm{s}}i_{\mathrm{d1}} + L_{\mathrm{q}}\omega_{\mathrm{e}}i_{\mathrm{q1}}\right) + \frac{p}{J_{\mathrm{tot}}L_{\mathrm{q}}}[K_{\mathrm{e}} + \left(L_{\mathrm{d}} - L_{\mathrm{q}}\right)i_{\mathrm{d1}}]\left(L_{\mathrm{d}}\omega_{\mathrm{e}}i_{\mathrm{d1}} + R_{\mathrm{s}}i_{\mathrm{q1}} + \omega_{\mathrm{e}}K_{\mathrm{e}}\right) + \omega_{\mathrm{m}} - \omega_{\mathrm{m}}^*\right\}\\ &= (i_{\mathrm{d1}} - i_{\mathrm{d1}}^*)\left(\frac{1}{L_{\mathrm{d}}}u_1 - \frac{R_{\mathrm{s}}}{L_{\mathrm{d}}}i_{\mathrm{d1}} + \frac{\omega_{\mathrm{e}}L_{\mathrm{q}}}{L_{\mathrm{d}}}i_{\mathrm{q1}} - \dot{i}_{\mathrm{d1}}^*\right) + \left(\frac{T_{\mathrm{m}}-T_{\mathrm{e}}}{J_{\mathrm{tot}}} - \dot{\omega}_{\mathrm{m}}^*\right)\left\{-\ddot{\omega}_{\mathrm{m}}^* - \frac{pi_{\mathrm{q1}}}{J_{\mathrm{tot}}L_{\mathrm{d}}}\left(L_{\mathrm{d}} - L_{\mathrm{q}}\right)u_1 - \frac{p}{J_{\mathrm{tot}}L_{\mathrm{q}}}[K_{\mathrm{e}} + \left(L_{\mathrm{d}} - L_{\mathrm{q}}\right)i_{\mathrm{d1}}]u_2 + \frac{\dot{T}_{\mathrm{m}}}{J_{\mathrm{tot}}} - \frac{pi_{\mathrm{q1}}}{J_{\mathrm{tot}}L_{\mathrm{d}}}\left(L_{\mathrm{d}} - L_{\mathrm{q}}\right)\left(-R_{\mathrm{s}}i_{\mathrm{d1}} +\right.\right.\end{aligned}$$

$$L_q\omega_e i_{q1}\big)+\frac{p}{J_{tot}L_q}\big[K_e+(L_d-L_q)i_{d1}\big](L_d\omega_e i_{d1}+\omega_e K_e)+\frac{R_s}{J_{tot}L_q}T_e+\omega_m-\omega_m^*\Big\} \quad (24)$$

Design PBLFC for system (17) as

$$\begin{cases} u_1=-\omega_e L_q i_{q1}+R_s i_{d1}^*+L_d\dot{i}_{d1}^*+v_1 \\ u_2=-\frac{L_q i_{q1}(L_d-L_q)}{L_d[K_e+(L_d-L_q)i_{d1}]}u_1+\frac{J_{tot}L_q}{p[K_e+(L_d-L_q)i_{d1}]}\{\ddot{\omega}_m^* \\ \quad -\frac{\dot{T}_m}{J_{tot}}+\frac{pi_{q1}}{J_{tot}L_d}(L_d-L_q)(-R_s i_{d1}+L_q\omega_e i_{q1}) \\ \quad -\frac{p}{J_{tot}L_q}\big[K_e+(L_d-L_q)i_{d1}\big](L_d\omega_e i_{d1}+\omega_e K_e) \\ \quad -\frac{R_s}{J_{tot}L_q}T_m+\frac{R_s}{L_q}\dot{\omega}_m^*-\omega_m+\omega_m^*+v_2\} \end{cases} \quad (25)$$

where auxiliary inputs v_1 and v_2 are designed as follows:

$$v_1=-\alpha_{11}(i_{d1}-i_{d1}^*) \quad (26)$$

$$v_2=-\alpha_{21}(\dot{\omega}_m-\dot{\omega}_m^*)-\alpha_{22}(\omega_m-\omega_m^*) \quad (27)$$

with positive constants α_{11}, α_{21}, and α_{22} being the linear feedback control gains of generator-side VSC.

3.3 Grid-side VSC control design

The control design of grid-side VSC attempts to enhance the FRT capability, i.e., reducing the magnitude and variation of the grid-side current and DC-link voltage while limiting them within their safety boundaries, under grid-side voltage dips and variable wind power inputs.

Define the tracking error $e'=[e_1', e_2']^T=[i_{q2}-i_{q2}^*, V_{dc}-V_{dc}^*]^T$, with i_{q2}^* and V_{dc}^* being the references of q-axis current and DC-link voltage, respectively. Differentiate the tracking error until the control input $u'=[u_1', u_2']^T=[V_{d2}, V_{q2}]^T$ appears explicitly, yields

$$\begin{bmatrix}\dot{e}_1'\\ \ddot{e}_2'\end{bmatrix}=\begin{bmatrix}f_1'(x)\\ f_2'(x)\end{bmatrix}+B_2(x)\begin{bmatrix}u_1'\\ u_2'\end{bmatrix}-\begin{bmatrix}\dot{i}_{q2}^*\\ \ddot{V}_{dc}^*\end{bmatrix} \quad (28)$$

where

$$f_1'(x)=-\frac{R_g}{L_g}i_{q2}-\omega_g i_{d2} \quad (29)$$

$$f_2'(x)=-\frac{3E_d}{2CV_{dc}}\left(\frac{1}{L_g}E_d-\frac{R_g}{L_g}i_{d2}+\omega_g i_{q2}\right)+\frac{3i_{d2}E_d}{2CV_{dc}^2}\left(\frac{1}{C}I_{dc1}-\frac{3E_d i_{d2}}{2CV_{dc}}\right)+\frac{1}{C}\dot{I}_{dc1} \quad (30)$$

with

$$B_2(x)=\begin{bmatrix}0 & -\frac{1}{L_g}\\ -\frac{3E_d}{2CL_gV_{dc}} & 0\end{bmatrix} \quad (31)$$

The inverse of control gain matrix $B_2(x)$ can be calculated as follows:

$$B_2^{-1}(x)=\begin{bmatrix}0 & -\frac{2CL_gV_{dc}}{3E_d}\\ -L_g & 0\end{bmatrix} \quad (32)$$

Similarly, the control gain matrix $B_2(x)$ must be nonsingular among the whole operation range to guarantee the above input-output linearization to be valid, requires

$$\det[B_2(x)]=-\frac{3E_d}{2CV_{dc}L_g^2}\neq 0 \quad (33)$$

which can be always satisfied when $E_d\neq 0$.

For system (28), construct a storage function as follows:

$$H_2=\underbrace{\frac{1}{2}\left(i_{q2}-i_{q2}^*\right)^2}_{\text{AC series-resistor heat}}+\underbrace{\frac{1}{2}(V_{dc}-V_{dc}^*)^2}_{\text{DC parallel-resistor heat}}+\underbrace{\frac{1}{2}\left(\frac{I_{dc}}{C}-\dot{V}_{dc}^*\right)^2}_{\text{DC series-resistor heat}} \quad (34)$$

Here, H_2 is constructed in the form of the sum of the heat produced by q-axis current i_{q2} flowing through an AC series virtual unit resistor, the heat produced by DC-link voltage V_{dc} across a DC parallel virtual unit resistor, and the heat produced by DC-link current I_{dc} flowing through a DC series virtual unit resistor associated with DC-link capacitor, respectively.

Remark 2. Similarly, the tracking error and storage function H_2 only include the q-axis current i_{q2} and DC-link voltage V_{dc} while d-axis current i_{d2} is excluded. This is due to the reason that FRT is achieved by regulating DC-link voltage V_{dc} (with relative degree of 2); While another goal is to regulate the reactive power which is determined by the q-axis current i_{q2} in the chosen alignment framework (with relative degree of 1). As there are only two inputs, e.g., u_1' and u_2', and the overall order of tracking error dynamics is 3, they are fully used to achieve the above two goals (2+1=3) and no more input could be adopted for the regulation of d-axis current i_{d2}. However, based on the relationship (10)-(12), d-axis current will be indirectly regulated after the q-axis current and DC-link voltage are all controlled.

Differentiate storage function H_2 (34) using Eq. (12) and Eqs. (28)-(31) with respect to the time, yields

$$\begin{aligned}\dot{H}_2&=\left(i_{q2}-i_{q2}^*\right)\left(\dot{i}_{q2}-\dot{i}_{q2}^*\right)+(V_{dc}-V_{dc}^*)\left(\tfrac{I_{dc}}{C}-\dot{V}_{dc}^*\right)+\left(\tfrac{I_{dc}}{C}-\dot{V}_{dc}^*\right)\left(\tfrac{\dot{I}_{dc}}{C}-\ddot{V}_{dc}^*\right)\\ &=\left(i_{q2}-i_{q2}^*\right)\left(\dot{i}_{q2}-\dot{i}_{q2}^*\right)+\left(\tfrac{I_{dc}}{C}-\dot{V}_{dc}^*\right)\left(\ddot{V}_{dc}-\ddot{V}_{dc}^*+V_{dc}-V_{dc}^*\right)\\ &=\left(i_{q2}-i_{q2}^*\right)\left(-\frac{1}{L_g}u_2'-\frac{R_g}{L_g}i_{q2}-\omega_g i_{d2}-\dot{i}_{q2}^*\right)+\\ &\left(\tfrac{I_{dc}}{C}-\dot{V}_{dc}^*\right)\left[-\ddot{V}_{dc}^*+V_{dc}-V_{dc}^*-\frac{3E_d}{2CV_{dc}}\left(\frac{1}{L_g}E_d-\frac{R_g}{L_g}i_{d2}+\omega_g i_{q2}\right)+\frac{3i_{d2}E_d}{2CV_{dc}^2}\left(\frac{1}{C}I_{dc1}-\frac{3E_d i_{d2}}{2CV_{dc}}\right)+\frac{1}{C}\dot{I}_{dc1}-\frac{3E_d}{2CL_gV_{dc}}u_1'\right]\\ &=\left(i_{q2}-i_{q2}^*\right)\left(-\frac{1}{L_g}u_2'-\frac{R_g}{L_g}i_{q2}-\omega_g i_{d2}-\dot{i}_{q2}^*\right)+\\ &\left(\tfrac{I_{dc}}{C}-\dot{V}_{dc}^*\right)\left[-\ddot{V}_{dc}^*+V_{dc}-V_{dc}^*-\frac{3E_d}{2CV_{dc}}\left(\frac{1}{L_g}E_d-\frac{R_g}{L_g}i_{d2}+\omega_g i_{q2}\right)+\frac{3i_{d2}E_d}{2CV_{dc}^2}\dot{V}_{dc}+\frac{1}{C}\dot{I}_{dc1}-\frac{3E_d}{2CL_gV_{dc}}u_1'\right]\end{aligned} \quad (35)$$

Design PBLFC for system (28) as

$$\begin{cases} u_1'=-\frac{2CL_gV_{dc}}{3E_d}[\ddot{V}_{dc}^*-V_{dc}+V_{dc}^*-\frac{1}{C}\dot{I}_{dc1}+\\ \frac{3E_d}{2CV_{dc}}\left(\frac{1}{L_g}E_d-\frac{R_g}{L_g}i_{d2}+\omega_g i_{q2}\right)-\frac{3i_{d2}E_d}{2CV_{dc}^2}\dot{V}_{dc}+v_1'] \\ u_2'=-L_g\dot{i}_{q2}^*-\omega_g L_g i_{d2}-R_g i_{q2}^*-v_2' \end{cases} \quad (36)$$

where auxiliary inputs v_1' and v_2' are designed in the linear state feedback form, as follows:

$$v_1'=-\alpha_{11}'\left(\dot{V}_{dc}-\dot{V}_{dc}^*\right)-\alpha_{12}'(V_{dc}-V_{dc}^*) \quad (37)$$

$$v_2'=-\alpha_{21}'\left(i_{q2}-i_{q2}^*\right) \quad (38)$$

with positive constants α_{11}', α_{12}', and α_{21}' being the linear feedback control gains of grid-side VSC.

3.4 Overall control structure

To this end, the overall control structure of PBLFC for PMSG based WECS is schematically described by Fig. 2.

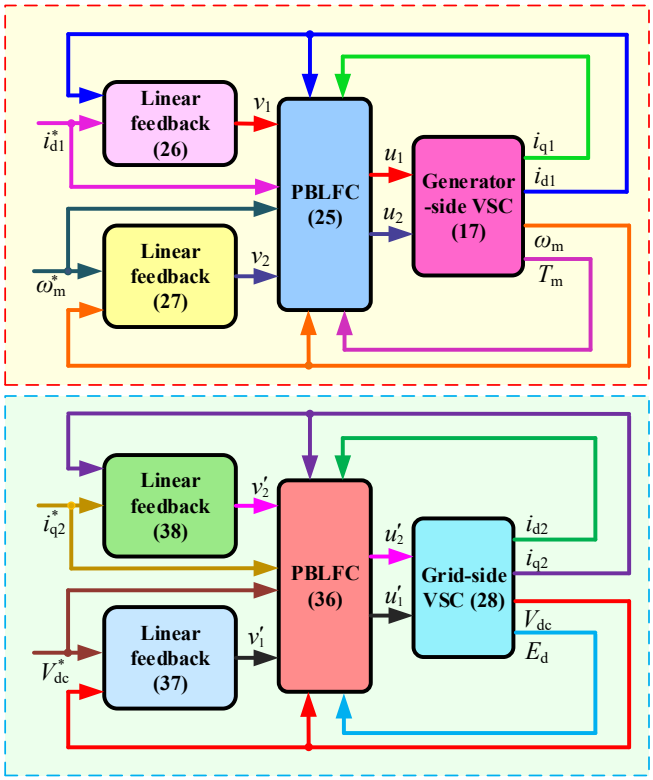

Figure 2. The overall control structure of PBLFC for PMSG based WECS.

4. Closed-loop System Analysis

This section aims to analyze the physical property and stability of the closed-loop system, such that a thorough interpretation of PBLFC can be achieved.

4.1. Generator-side VSC analysis

Substitute PBLFC (25) into the derivative of storage function (24), together with the electromechanical relationship (8), gives

$$\dot{H}_1 = \underbrace{-\frac{R_s}{L_d}(i_{d1}-i_{d1}^*)^2 - \frac{R_s}{L_q}(\dot{\omega}_m-\dot{\omega}_m^*)^2}_{\text{beneficial terms}} + \underbrace{\frac{i_{d1}-i_{d1}^*}{L_d}v_1 + (\dot{\omega}_m-\dot{\omega}_m^*)v_2}_{\text{auxiliary inputs}} \tag{39}$$

The first two terms of system (39) are carefully remained as they are beneficial terms which can accelerate the tracking error rate of d-axis current i_{d1} and mechanical rotation speed ω_m. In particular, their physical property can be interpreted as the sum of the heat produced by the d-axis current i_{d1} on the stator resistance R_s associated with d-axis inductance L_d and the acceleration torque energy associated with the stator resistance R_s and q-axis inductance L_q, such energy will be dissipated rapidly through manipulating the auxiliary inputs to accelerate the decrease rate of storage function, that is, a larger system damping.

The closed-loop system of generator-side VSC is obtained by substituting PBLFC (25) into tracking error dynamics (17), yields

$$\begin{cases} \dot{e}_1 + \frac{R_s+\alpha_{11}}{L_d}e_1 = 0 \\ \ddot{e}_2 + \left(\frac{R_s}{L_q}+\alpha_{21}\right)\dot{e}_2 + (1+\alpha_{22})e_2 = 0 \end{cases} \tag{40}$$

From the closed-loop system (40), it can be found that its poles are located at $-\left(\frac{R_s+\alpha_{11}}{L_d}\right)$ and $-\frac{1}{2}\left(\frac{R_s}{L_q}+\alpha_{21}\right) \pm \frac{1}{2}\sqrt{\left(\frac{R_s}{L_q}+\alpha_{21}\right)^2 - 4(1+\alpha_{22})}$ for d-axis current and mechanical rotation speed, respectively.

4.2. Grid-side VSC analysis

Substitute PBLFC (36) into the derivative of storage function (35), together with the voltage-current relationship of DC-link (13), yields

$$\dot{H}_2 = \underbrace{-\frac{R_g}{L_g}\left(i_{q2}-i_{q2}^*\right)^2}_{\text{beneficial terms}} + \underbrace{\frac{i_{q2}-i_{q2}^*}{L_g}v_2' + \left(\dot{V}_{dc}-\dot{V}_{dc}^*\right)v_1'}_{\text{auxiliary inputs}} \tag{41}$$

Similarly, the first term of system (41) are carefully remained as they are beneficial terms which can accelerate the tracking error rate of q-axis current i_{q2} and DC-link voltage V_{dc}. Here, their physical meaning can be interpreted as the sum of the heat produced by the q-axis current i_{q2} on the grid resistance R_g associated with grid inductance L_g.

Meanwhile, the closed-loop system of grid-side VSC is obtained through substituting PBLFC (36) into tracking error dynamics (28), gives

$$\begin{cases} \dot{e}_1' + \frac{R_g+\alpha_{21}'}{L_g}e_1' = 0 \\ \ddot{e}_2' + \alpha_{11}'\dot{e}_2' + (1+\alpha_{12}')e_2' = 0 \end{cases} \tag{42}$$

From the closed-loop system (42), it can be found that its poles are located at $-\left(\frac{R_g+\alpha_{21}'}{L_i}\right)$ and $-\frac{1}{2}\alpha_{11}' \pm \frac{1}{2}\sqrt{\alpha_{11}'^2 - 4(1+\alpha_{12}')}$ for q-axis current and DC-link voltage, respectively.

Remark 3. The third term of H_1, e.g., $\frac{1}{2}\left(\frac{T_m-T_e}{J_{tot}} - \dot{\omega}_m^*\right)^2$ and the third term of H_2, e.g., $\frac{1}{2}\left(\frac{I_{dc}}{C} - \dot{V}_{dc}^*\right)^2$ are actually $\frac{1}{2}(\dot{\omega}_m - \dot{\omega}_m^*)^2$ and $\frac{1}{2}(\dot{V}_{dc} - \dot{V}_{dc}^*)^2$. This can be directly obtained from the relationship of $J_{tot}\frac{d\omega_m}{dt} = T_m - T_e$ and $C\frac{dV_{dc}}{dt} = I_{dc}$. The reason this paper does not directly use their derivative but indirectly use their equivalent relationship is to provide a clearer physical representation of these two terms. More specifically, one can find the mechanical torque T_m, electromagnetic torque T_e, and total inertia of the drive train J_{tot} of H_1 as they can be directly measured/obtained in practice; Similarly, one can find the DC-link current I_{dc} and DC-link capacitor C of H_2 as they can be directly measured/obtained in practice.

Remark. 4 PBLFC can noticeably improve the transient responses of PMSG based WECS thanks to the beneficial terms retained through passivity analysis [16]. In contrast, FLC [6,9] fully removes all the terms regardless of their actual roles. Moreover, as PBLFC offers a clear physical meaning and employs the typical linear feedback control framework, it is relatively easy to be accepted in both industry and academics.

4.3. Overall closed-loop system roots

From the above discussion, one can readily obtain that these roots are all located at left-half plane (LHP) thus the closed-loop system is asymptotically stable. Here, Fig. 3 clearly demonstrates the location of all possible roots of the closed-loop systems (40) and (42), in which the linear feedback control gains mainly determine the tracking error dynamics, while other system parameter related components are beneficial terms remained via passivity analysis. The roots are given as follows:

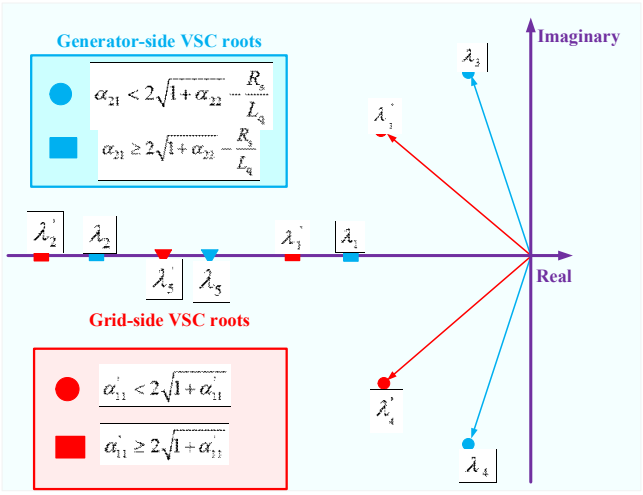

Figure 3. The roots of the closed-loop system.

$$\begin{cases} \lambda_{1,2} = -\frac{1}{2}\left(\frac{R_s}{L_q}+\alpha_{21}\right) \pm \frac{1}{2}\sqrt{\left(\frac{R_s}{L_q}+\alpha_{21}\right)^2 - 4(1+\alpha_{22})} \\ \lambda'_{1,2} = -\frac{1}{2}\alpha'_{11} \pm \frac{1}{2}\sqrt{\alpha'^{\,2}_{11} - 4(1+\alpha'_{12})} \\ \lambda_{3,4} = -\frac{1}{2}\left(\frac{R_s}{L_q}+\alpha_{21}\right) \pm j\frac{1}{2}\sqrt{4(1+\alpha_{22}) - \left(\frac{R_s}{L_q}+\alpha_{21}\right)^2} \\ \lambda'_{3,4} = -\frac{1}{2}\alpha'_{11} \pm j\frac{1}{2}\sqrt{4(1+\alpha'_{12}) - \alpha'^{\,2}_{11}} \\ \lambda_5 = -\frac{R_s+\alpha_{11}}{L_d} \\ \lambda'_5 = -\frac{R_g+\alpha'_{21}}{L_g} \end{cases} \quad (43)$$

5. Case Studies

The proposed PBLFC is applied on PMSG based WECS, which control performance is compared to that of conventional VC [8] and FLC [9], under three cases, e.g., (a) Step change of wind speed; (b) Stochastic wind speed variation; and (c) Fault ride-through. Consider the control inputs may exceed the admissible capacity of VSC at some operation points, therefore their values must be limited. Here, u_1, u_2, u'_1, and u'_2 are all bounded among [-0.65, 0.65] per unit (p.u.). Moreover, the PMSG based WECS parameters and PBLFC parameters are tabulated in Table 1 [9], [13] and Table 2, respectively.

It is worth noting that the MPPT and FRT are tested independently as they are in different time-scale. More specifically, For the MPPT at generator side, it assumes there's no fault at GSC side and the goal just focuses on the MPPT; For the FRT at grid side, its time-scale is just less than 0.3s. During such short period of time the wind speed could be assumed to be a constant thus one can focus on FRT only.

Note that a larger value of control parameters in Table 2 will result in a faster tracking rate but also higher control costs; while a smaller value will lead to a slower tracking rate but also lower control costs. Therefore, the control parameters are determined by trial-and-error to achieve a proper trade-off between the tracking rate and control costs. Lastly, the simulation is executed on Matlab/Simulink 7.10 using a personal computer with an Intel^R CoreTMi7 CPU at 2.2 GHz and 8 GB of RAM.

Table 1. The PMSG based WECS parameters

PMSG rated power	$\boldsymbol{P_{base}}$	2 MW	Field flux	$\boldsymbol{K_e}$	136.25 V·s/rad
Radius of wind turbine	R	39 m	Pole pairs	p	11
Grid-side VSC resistance	R_g	125 mΩ	Grid-side VSC inductance	L_g	18.5 mH
d-axis stator inductance	L_d	5.5 mH	Air density	ρ	1.205 kg/m^3
q-axis stator inductance	L_q	3.75 mH	Rated wind speed	v_{wind}	12 m/s
Total inertia	J_{tot}	10000 kg·m^2	Stator resistance	R_s	40 mΩ
DC-link capacitor	C	134 mF	Grid angular speed	ω_g	100π rad/s
DC-link voltage	V_{dc}	1500 V	Grid voltage	E	690 V
Switch frequency	f	1620 Hz			

Table 2. The PBLFC parameters

Generator-side VSC	$\boldsymbol{\alpha_{11}}$= 20	$\boldsymbol{\alpha_{21}}$=40	$\boldsymbol{\alpha_{22}}$=120
Grid-side VSC	α'_{11}=30	α'_{12}=80	α'_{21}=25

5.1. Step change of wind speed

Four consecutive step changes of wind speed from 8 m/s to 12 m/s with a 10 m/s^2 rate are adopted to evaluate the MPPT performance of each controller. Meanwhile, two step changes of d-axis current reference are also used to test the d-axis current regulation performance. Fig. 4 clearly exhibits the system responses, which shows that VC owns the highest overshoot of active power during MPPT, the lowest tracking rate against that of FLC and PBLFC, as well as significant control performance degradation when operation condition varies resulted from one-point linearization. In contrast, both FLC and PBLFC are able to realize a consistent control performance at different operation conditions thanks to the compensation of PMSG nonlinearities. Furthermore, the power coefficient of PBLFC is the closest to the optimal value thus it can extract the maximum power from wind. While PBLFC outperforms FLC in terms of faster tracking rate and smaller overshoot as the physical property of PMSG is beneficially exploited. At last, one can observe that PBFLC is able to rapidly regulate the d-axis current without any overshoot. Besides, the DC link voltage and grid side current demonstrate that PBFLC can track their references with the fastest rate and smallest overshoot, thus it can provide the most satisfactory control performance in both generator side and grid side.

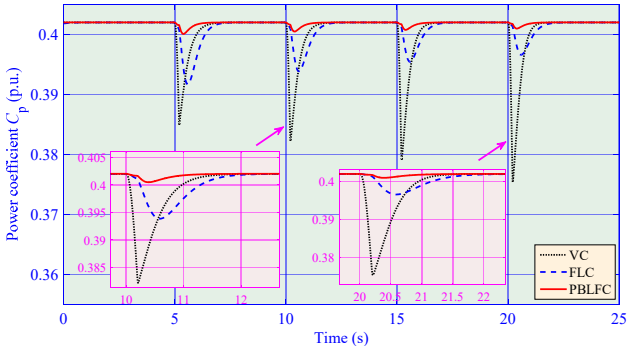

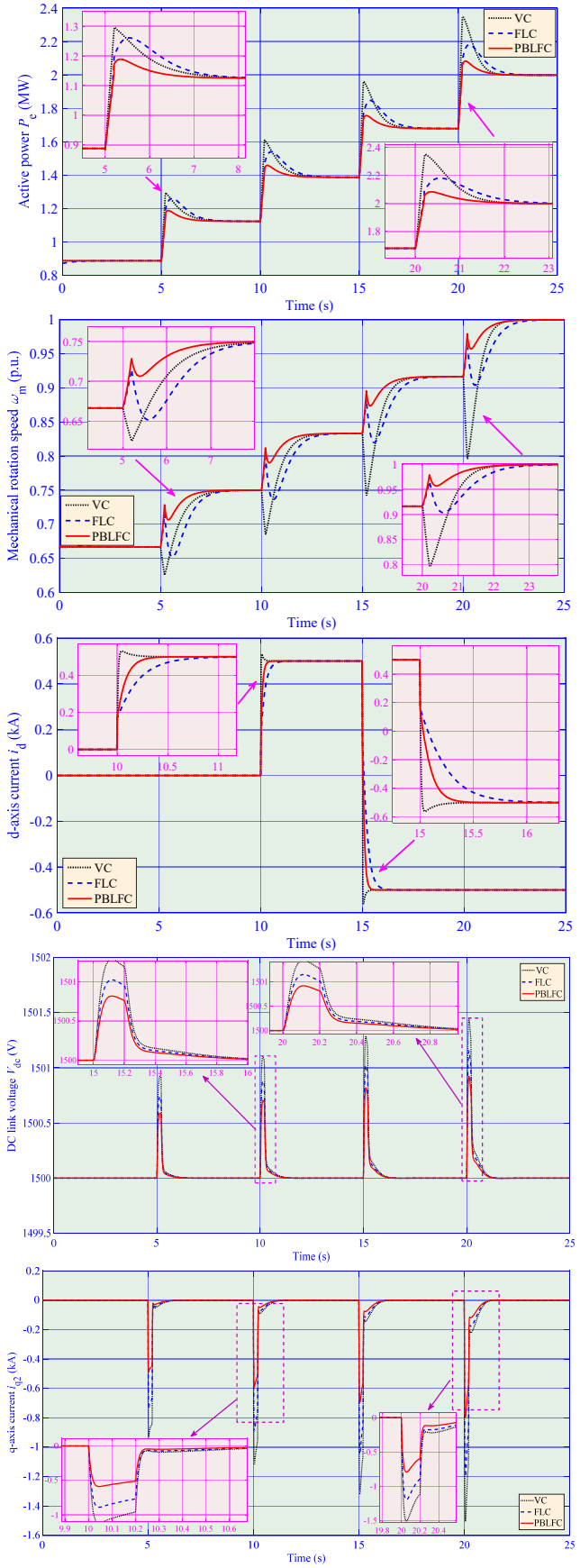

Figure 4. System responses and control costs obtained under a step change of wind speed from 8 m/s to 12 m/s.

5.2. Stochastic wind speed variation

It is well known that wind speed is highly random and intermittent in nature [25]. In order to mimic a more general and realistic wind variation in practice, a stochastic wind speed variation starts from 6 m/s and ends at 12 m/s is applied to evaluate the control performance of each control schemes. The system responses are given in Fig. 5, which presents that PBFLC can always keep its power coefficient to be the closest to the optimum at the fastest speed. Hence it can offer the best MPPT performance among all approaches. In contrast, the control performance of VC varies considerably under such severe wind speed variation. The grid side results also demonstrate that PBFLC can effectively regulate the DC link voltage and grid side current and outperform that of others under the stochastic wind speed variation.

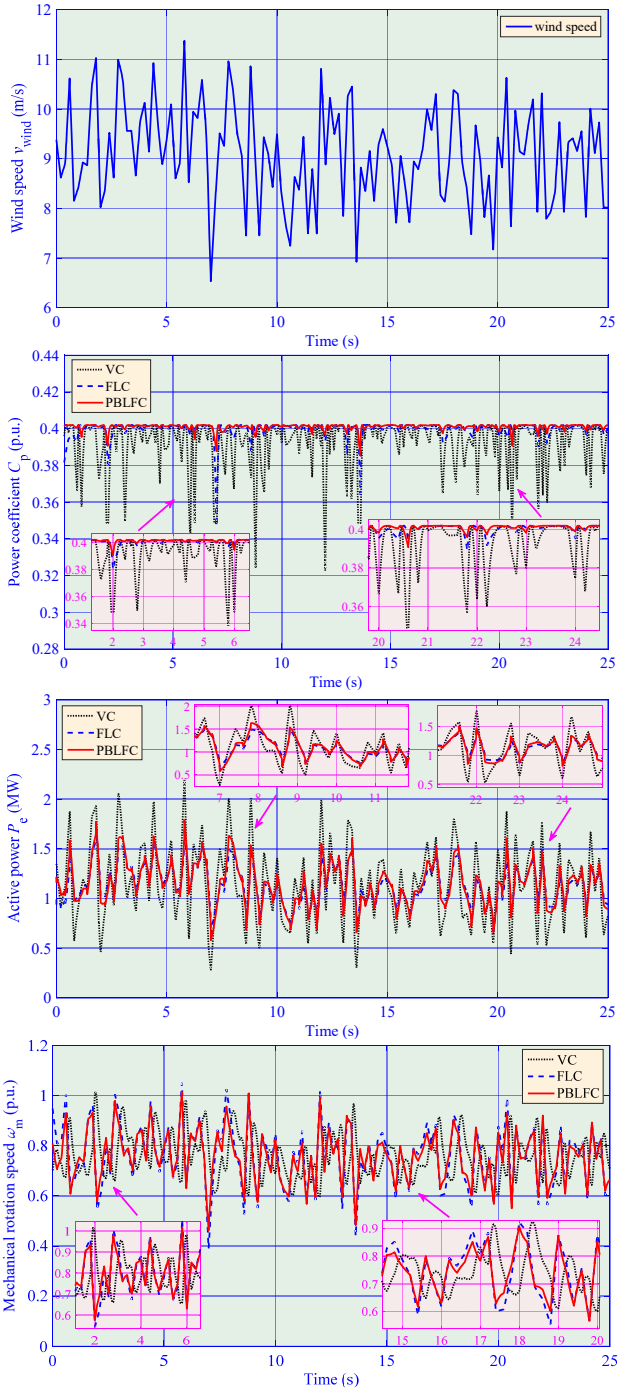

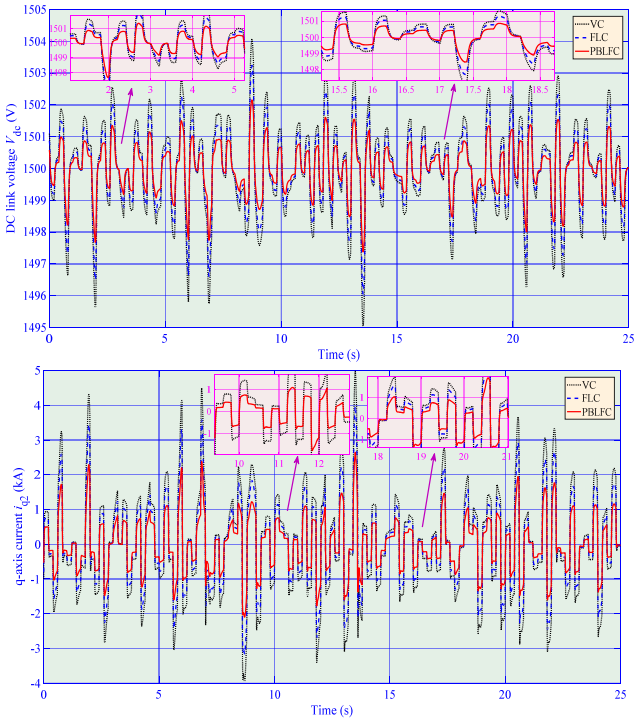

Figure 5. System responses obtained under a stochastic wind speed variation from 6 m/s to 12 m/s.

5.3. Fault ride-through

FRT requires the PMSG to be remained connected to the power grid during and after grid faults, or undergoes voltage dips caused by load disturbances, and provides active/reactive power control to the power grid. A 30 % voltage dip lasting 0.2 s is applied on power grid while q-axis current is regulated at 0 to maintain a unit power factor [31]. Besides, The strategy C proposed in references [32,33] is adopted for comparison of FRT as well, which is based on a simple concept to transform the unbalanced energy into the kinetic one, rather than being dissipated otherwise. For the grid side control scheme, a compensation item, which reflects the variation of the DC-link current of the generator side converter, is added during the fault to smooth the fluctuations of the DC-link voltage.The FRT performance of each controller is displayed in Fig. 6. One can find that PBLFC can effectively regulate both the DC-link voltage and q-axis current with the smallest overshoot and fastest convergence rate, thus it can provide the highest FRT capability among all methods. Moreover, strategy C can improve the FRT compares to that of VC and FLC thanks to its novel mechanism with a rapid restoration of the disturbed PMSG system as well as a lower overshoot of DC link voltage.

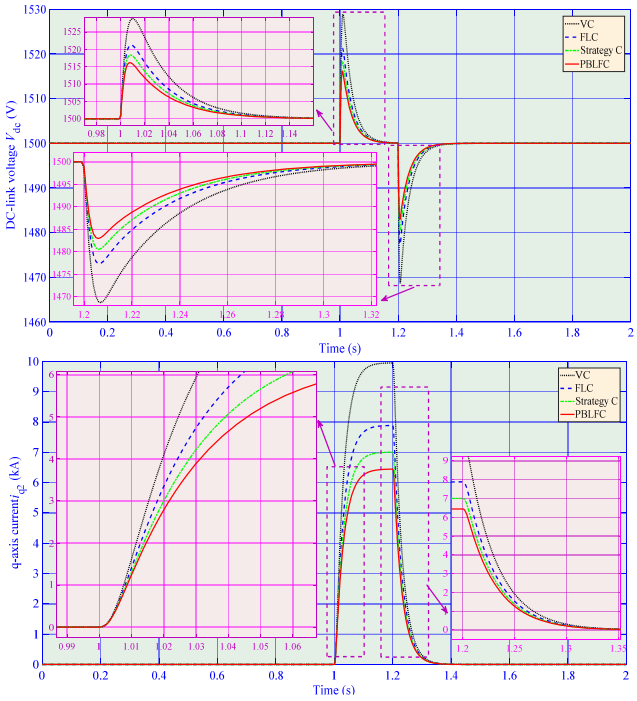

Figure 6. FRT performance obtained under a 30% voltage dip lasting 0.2 s at power grid.

5.4. Comparative studies

The real-time variation of the summed storage function $H=H_1+H_2$ is recorded in Fig. 7, from which one can determine the tracking error by examining the slope of the curve, i.e., a steeper slope indicates a faster tracking error. It is clear that PBLFC owns the fastest tracking rate, together with the lowest peak value (tracking error overshoot).

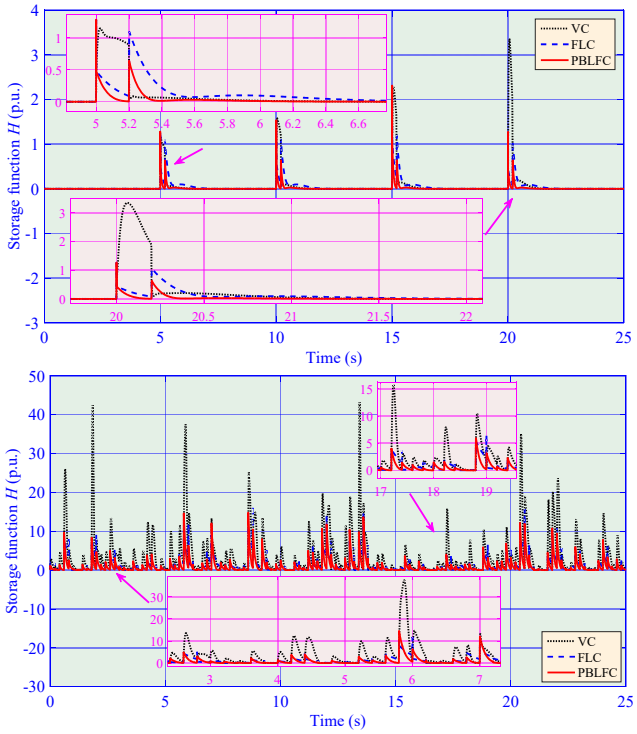

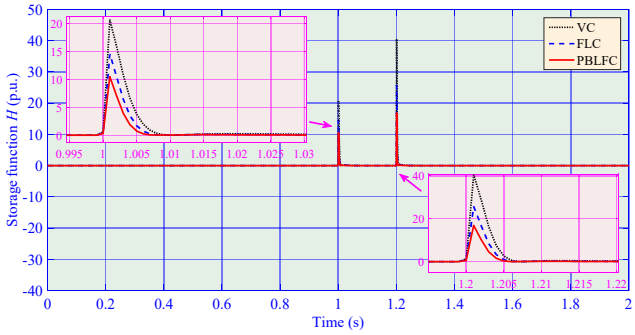

Figure 7. The real-time variation of the summed storage function *H*.

Moreover, the integral of the sum of two storage functions of different cases, e.g., $\int_0^T(|H_1|+|H_2|)\mathrm{d}t$, are provided by Fig. 8, which evaluates the overall storage energy generated by the tracking error while a smaller value indicates a lower overall tracking error. Obviously, PBLFC offers the lowest overall tracking error in all three cases.

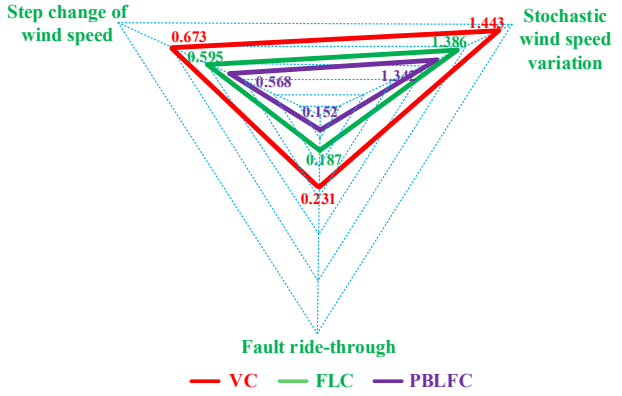

Figure 8. The radar diagram of integral of the sum of two storage functions calculated under three cases.

Lastly, the overall control costs, e.g., $\int_0^T(|u_1|+|u_2|+|u_1'|+|u_2'|)\mathrm{d}t$, of all controllers required in three cases are compared in Fig. 9. It can be readily seen that PBLFC just requires the minial control costs in all cases among all controllers thanks to the beneficial exploitation of physical property of PMSG based WECS.

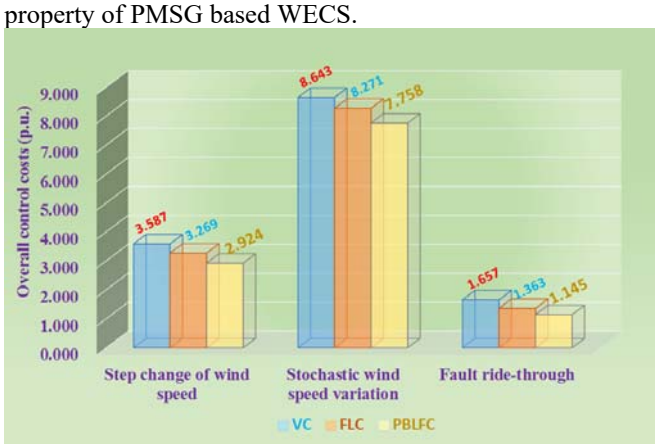

Figure 9. Overall control costs obtained by different controllers under three cases.

6. Conclusions

In this paper, a PBLFC scheme is designed for PMSG based WECS. The main contributions can be summarized in the following three points:

(i) A storage function is constructed based on the passivity theory, in which the actual role of each term is investigated in details. Meanwhile, the beneficial terms are retained such that the transient responses of PMSG can be considerably improved. Furthermore, linear feedback control is employed as an additional input to guarantee a desired tracking error convergence;

(ii) The closed-loop system stability is thoroughly analyzed, in which all possible roots are calculated, together with a clear physical interpretation of the storage function. Hence, it is easy to be understood and accepted by both industry and academics;

(iii) Simulation results of three case studies demonstrate that PBLFC can achieve a globally consistent control performance and achieve MPPT under various wind speed, noticeably enhance the FRT capability, and require just minimal overall control costs compared to that of VC and FLC.

Future studies will employ some typical meta-heuristic algorithms to assign the optimal system roots via optimal control parameters tunning, such that an optimal control performance of PMSG based WECS can be achieved by PBLFC.

Acknowledgments

The authors gratefully acknowledge the support of National Natural Science Foundation of China (51477055, 51667010, 51777078).

References

[1] Liao, S.W.; Yao, W.; Han, X.N.; Wen, J.Y.; Cheng, S.J. Chronological operation simulation framework for regional power system under high penetration of renewable energy using meteorological data. *Applied Energy* **2017**, 203: 816-828.

[2] Yao, W.; Jiang, L.; Wen, J.Y.; Wu, Q.H.; Cheng, S.J. Wide-area damping controller for power system inter-area oscillations: a networked predictive control approach. *IEEE Transactions on Control Systems Technology* **2015**, 23(1): 27-36.

[3] Yang, B.; Jiang, L.; Wang, L.; Yao, W.; Wu, Q.H. Nonlinear maximum power point tracking control and modal analysis of DFIG based wind turbine. *International Journal of Electrical Power and Energy Systems* **2016**, 74: 429-436.

[4] Yang, B.; Zhang, X.S.; Yu, T.; Shu, H.C.; Fang, Z.H. Grouped grey wolf optimizer for maximum power point tracking of doubly-fed induction generator based wind turbine. *Energy Conversion and Management* **2017**, 133, 427-443.

[5] Yao, J.; Yu, M.; Gao, W.; Zeng, X. Frequency regulation control strategy for PMSG wind-power generation system with flywheel energy storage unit. *IET Renewable Power Generation* **2017**, 11(8):1082-1093.

[6] Youcef, S.; Sami, K.; Mohcene, B. Feedback linearization control based particle swarm optimization for maximum power point tracking of wind turbine equipped by PMSG connected to the grid. *International Journal of Hydrogen Energy* **2016**, 41, 20950-20955.

[7] Yao, J.; Guo, L.; Zhou, T.; Xu, D.; Liu, R. Capacity configuration and coordinated operation of a hybrid wind farm with FSIG-based and PMSG-based wind farms during grid faults, *IEEE Transactions on Energy Conversion* **2017**, 32(3), 1188-1199.

[8] Shehata, E.G. A comparative study of current control schemes for a direct-driven PMSG wind energy generation system. *Electric Power Systems Research* **2017**, 143, 197-205.

[9] Chen, J.; Jiang, L.; Yao, W.; Wu, Q.H. A feedback linearization control strategy for maximum power point tracking of a PMSG based wind turbine. International Conference on Renewable Energy Research and Applications, Madrid, Spain, 20-23 October 2013, 79-84.

[10] Seyed, M.M.; Maarouf, S.; Hani, V.; Handy, F.B.; Mohsen, S. Sliding mode control of PMSG wind turbine based on enhanced exponential reaching law. *IEEE Transactions on Industrial Electronics* **2016**, 63(10), 6148-6159.

[11] Riad, A.; Toufik, R.; Djamila, R.; Abdelmounaim, T. Application of nonlinear predictive control for charging the battery using wind energy with permanent magnet synchronous generator. *International Journal of Hydrogen Energy* **2016**, 41, 20964-20973.

[12] Fantino, R.; Solsona, J.; Busada, C. Nonlinear observer-based control for PMSG wind turbine. *Energy* **2016**, 113, 248-257.

[13] Chen, J.; Jiang, L.; Yao, W.; Wu, Q. H. Perturbation estimation based nonlinear adaptive control of a full-rated converter wind turbine for fault ride-through capability enhancement. *IEEE Transactions on Power Systems* **2014**, 29(6), 2733-2743.

[14] Yassin, H.M.; Hanafy, H.H.; Hallouda, M.M. Enhancement low-voltage ride through capability of permanent magnet synchronous generator-based wind turbines using interval type-2 fuzzy control. *IET Renewable Power Generation* **2016**, 10(3), 339-348.

[15] Li, S.Q.; Zhang, K.Z.; Li, J.; Liu, C. On the rejection of internal and external disturbances in a wind energy conversion system with direct-driven PMSG. *ISA Transactions* **2016**, 61, 95-103.

[16] Ortega, R.; Schaft, A.; Mareels, I.; Maschke, B. Putting energy back in control. *IEEE Control Systems* **2001**, 21(2), 18-33.

[17] Fernando, M.D.; Ortega, R. Adaptive passivity-based control for maximum power extraction of stand-alone windmill systems. *Control Engineering Practice* **2012**, 20, 173-181.

[18] Santos, G.V.; Cupertino, A.F.; Mendes, V.F.; Seleme, S.I. Interconnection and damping assignment passivity-based control of a PMSG based wind turbine for maximum power tracking. 2015 IEEE 24th International Symposium on Industrial Electronics (ISIE), Buzios, Brazil, 3-5 June, 2015, 306-311.

[19] Zheng, X.; Li, Q.; Ding, D.; Li, P.; Li, H. Passivity non-singular higher-order sliding mode control for direct-driven PMSG. IECON 2014 - 40th Annual Conference of the IEEE Industrial Electronics Society, Dallas, TX, USA, 29 Oct.-1 Nov. 2014, 5575-5581.

[20] Yang, B.; Yu, T.; Shu, H. C.; Zhang, Y. M.; Chen, J.; Sang, Y.Y.; Jiang, L. Passivity-based sliding-mode control design for optimal power extraction of a PMSG based variable speed wind turbine. *Renewable Energy* **2018**,119: 577-589.

[21] Jeong, D.; Kim, C.; Gui, Y.; Chung, C.C. Sliding mode control for LVRT of a PMSG wind turbine using stored energy in rotor inertia. 2016 IEEE Power and Energy Society General Meeting (PESGM), Boston, MA, USA, 17-21 July, p.1-5.

[22] Gui, Y.H.; Kim, C.H.; Chung C.C. Improved low-voltage ride through capability for PMSG wind turbine based on port-controlled Hamiltonian system. *International Journal of Control, Automation and Systems* **2016**,14(5): 1195-1204.

[23] Pahlevani, M.; Pan, S.; Mash, J.; Jain, P. Port-controlled Hamiltonian (PCH)-based control approach for wind energy conversion systems. 2014 IEEE 5th International Symposium on Power Electronics for Distributed Generation Systems (PEDG), Galway, Ireland, 24-27, June, 2014, p. 1-5.

[24] Valenciaga, F.; Puleston, P.F.; Battaiotto, E.; Mantz, R.J. Passivity/sliding mode control of a stand-alone hybrid generation system. *IEE Proceedings-Control Theory and Applications* **2000**, 147(6): 680-686.

[25] Fernando, V.; Pablo, F.P.; Pedro, E.B. Power control of a solar/wind generation system without wind measurement: a passivity/sliding mode approach. *IEEE Transactions on Energy Conversion* **2003**,18(4): 501-507.

[26] Cisneros, R.; Mancilla–David, F.; Ortega, R. Passivity-based control of a grid-connected small-scale windmill with limited control authority. *IEEE Journal of Emerging and Selected Topics in Power Electronics* **2013**, 1(4): 247-259.

[27] Croci, L.; Martinez, A.; Coirault, P.; Champenois, G.; Gaubert, J.P. Comparison of two Passivity-based control strategies for a wind power generator. Industrial Electronics Society, IECON 2013 - 39th Annual Conference of the IEEE, Vienna, Austria, 10-13, Nov. 2013, p. 5248-5253.

[28] Uehara, A.; Pratap, A.; Goya, T.; Senjyu, T.; Yona, A.; Urasaki, N.; Funabashi, T. A coordinated control method to smooth wind power fluctuations of a PMSG-based WECS. *IEEE Transactions on Energy Conversion* **2011**, 26(2), 550-558.

[29] Karakus, O.; Kuruoglu, E.; Altinkaya, M. One-Day ahead wind speed/power prediction based on polynomial autoregressive model. *IET Renewable Power Generation* **2017**, 11(11), 1430-1439.

[30] Shen, Y.; Yao, W.; Wen, J.Y.; He, H.B.; Chen, W.B. Adaptive supplementary damping control of VSC-HVDC for interarea oscillation using GrHDP. *IEEE Transactions on Power Systems* **2018**, 33(2): 1777-1789.

[31] Yang, B.; Yu, T.; Shu, H.C.; Zhang, X.S.; Qu, K.P.; Jiang, L. Democratic joint operations algorithm for optimal power extraction of PMSG based wind energy conversion system, *Energy Conversion and Management* **2018**, 159: 312-326.

[32] Yang, L.H.; Xu, Z.; Østergaard, J.; Dong, Z. Y.; Wong, K. P. Advanced control strategy of DFIG wind turbines for power system fault ride through. *IEEE Transactions on Power Systems* **2012**, 27(1): 713-722.

[33] Xie, D. L.; Xu, Z.; Yang, L.H.; Østergaard, J.; Xue, Y.S.; Wong, K.P. A comprehensive LVRT control strategy for DFIG wind turbines with enhanced reactive power support. *IEEE Transactions on Power Systems* **2013**, 28(3): 3302-3310.